View metadata, citation and similar papers at core.ac.uk

brought to you by CORE

provided by Elsevier - Publisher Connector

Biophysical Journal Volume 95 October 2008 4013–4024

Microarchitecture of Three-Dimensional Scaffolds Influences Cell Migration Behavior via Junction Interactions

Brendan A. C. Harley,* Hyung-Do Kim,† Muhammad H. Zaman,‡ Ioannis V. Yannas,*† Douglas A. Lauffenburger,† and Lorna J. Gibson§

*Department of Mechanical Engineering and †Department of Biological Engineering, Massachusetts Institute of Technology, Cambridge, Massachusetts; ‡Department of Biomedical Engineering, University of Texas, Austin, Texas; and §Department of Materials Science and Engineering, Massachusetts Institute of Technology, Cambridge, Massachusetts

ABSTRACT Cell migration plays a critical role in a wide variety of physiological and pathological phenomena as well as in scaffold-based tissue engineering. Cell migration behavior is known to be governed by biochemical stimuli and cellular interactions. Biophysical processes associated with interactions between the cell and its surrounding extracellular matrix may also play a significant role in regulating migration. Although biophysical properties of two-dimensional substrates have been shown to significantly influence cell migration, elucidating factors governing migration in a three-dimensional environment is a relatively new avenue of research. Here, we investigate the effect of the three-dimensional microstructure, specifically the pore size and Young's modulus, of collagen-glycosaminoglycan scaffolds on the migratory behavior of individual mouse fibroblasts. We observe that the fibroblast migration, characterized by motile fraction as well as locomotion speed, decreases as scaffold pore size increases across a range from 90 to 150 μm. Directly testing the effects of varying strut Young's modulus on cell motility showed a biphasic relationship between cell speed and strut modulus and also indicated that mechanical factors were not responsible for the observed effect of scaffold pore size on cell motility. Instead, in-depth analysis of cell locomotion paths revealed that the distribution of junction points between scaffold struts strongly modulates motility. Strut junction interactions affect local directional persistence as well as cell speed at and away from the junctions, providing a new biophysical mechanism for the governance of cell motility by the extracellular microstructure.

INTRODUCTION

Cell motility is critical in many physiological and pathological processes, as well as in tissue-engineering applications. Cell migration is modulated by a complex, spatiotemporally integrated set of biophysical mechanisms that are influenced not only by the biochemistry of extracellular and intracellular signaling, but also by the biophysics of the surrounding extracellular environment (1,2). Efforts in studying the effect of the extracellular environment on cell migratory behavior have led to an improved understanding of how substrate features, especially substrate stiffness, affect migration through changes in cytoskeletal organization and applied traction forces (3–5). However, the vast majority of studies probing cell-substrate interactions have done so using artificial two-dimensional surfaces. As a result, our understanding of the critical biochemical and biophysical parameters that affect cell motility in three-dimensional (3D) environments is quite limited. Extending such studies to the third dimension requires considering the in vivo extracellular environment in which cell behavior is regulated.

One of the main components of the 3D in vivo extracellular environment is the extracellular matrix (ECM), a complex network of structural matrix protein fibers and glycosaminoglycans (2). In addition to providing biochemical stimuli, the ECM provides three-dimensional microstructural and mechanical cues, both of which have been shown to significantly influence 3D cell migration in recent computational and experimental studies (6,7). In addition, heterogeneities within the 3D ECM, such as steric hindrances imposed on cell movement by the dense ECM network, may introduce geometry-dependent effects on migratory behavior (8,9); the fiber thickness and the pore size of an analog of this in vivo ECM microenvironment may play a role in regulating migratory behavior. Manipulation of ECM geometries on two-dimensional (2D) substrata using lithographic and microprinting techniques have demonstrated that microstructural guidance affects cell migration and its related cellular functions (10,11). Such ''contact guidance'' by the ECM has been demonstrated in vivo in recent intravital imaging studies of carcinoma cells in the mammary fat pad (12). These studies show preferential chemotactic movement of invasive carcinoma cells along thick collagen fibers toward blood vessels. In the lymph node paracortex, the porous microarchitecture of collagen and fibronectin bundles ensheathed by fibroblastic reticular cells has been shown to significantly influence T-cell migration behavior and is believed to facilitate colocalization of T-cells with dendritic cells (13). Contact guidance cues have also been observed governing T-cell motility through composite macroporous poly(ethylene glycol) hydrogel scaffolds infused with collagen in vitro (14).

Submitted September 21, 2007, and accepted for publication June 9, 2008.

Brendan A. C. Harley and Hyung-Do Kim contributed equally to this work.

Address reprint requests to L. J. Gibson, Dept. of Materials Science and Engineering, Massachusetts Institute of Technology, 77 Massachusetts Ave., Rm. 8-135, Cambridge, MA 02139. Tel.: 617-253-7107; Fax: 617-258-6275; E-mail: ljgibson@mit.edu.

Editor: Herbert Levine.

© 2008 by the Biophysical Society

0006-3495/08/10/4013/12 $2.00

doi: 10.1529/biophysj.107.122598

These studies indicate that in vivo and in vitro ECM geometries and microarchitecture play a significant role in modulating cell migration. However, it is still unknown how specific parameters of an ECM microstructure influence cell migration.

Three-dimensional tissue-engineering scaffolds are analogs of the ECM present in all tissues and organs. The scaffold acts as a physical support structure and insoluble regulator of cell activity. It should be noted that scaffold microstructure (porosity, mean pore size, pore shape, interconnectivity, specific surface area) (15–17) and mechanical properties (Young's modulus) (18–21) have been shown to significantly influence cell behaviors such as adhesion, growth, and differentiation, and to affect the bioactivity of scaffolds used for in vivo regeneration applications of various tissues, such as cartilage, skin, and peripheral nerves (22–24). Three-dimensional tissue engineering constructs provide a powerful model system for studying cell migration. For tissue engineering purposes, understanding extracellular influences on cell motility within physiologically relevant 3D constructs can aid the design of future bioactive constructs, since an initially acellular scaffold must be rapidly cellularized. Controlling cell motility by modulating the local engineered extracellular environment process is also a critical stepping stone in the development of the next generation of bioactive tissue engineering scaffolds. A homologous series of controlled scaffold microenvironments provides an ideal construct to explore the individual influence of specific extracellular cues on cell motility. However, quantitative study of individual cell behavior within a 3D scaffold construct requires understanding the local extracellular environment through compositional, microstructural, and mechanical characterization. In the past, the lack of standardized 3D constructs with well characterized and independently variable mechanical, compositional, and microstructural properties made it difficult to draw quantitative conclusions regarding the independent effect of the specific extracellular features on cell behavior.

In this investigation, we use highly porous collagen-glycosaminoglycan (CG) scaffolds fabricated through a freeze drying, or lyophilization, process as a model ECM system (25). These low-density, open-cell foams are biodegradable, are characterized by an interconnected pore network defined by fibers of collagen-GAG coprecipitate, termed ''struts'', and provide an ideal environment for in vitro cell behavior studies. CG scaffolds have previously been shown to possess physiologically relevant pore sizes, degradation rates, and chemical compositions when used to induce in vivo regeneration of skin and peripheral nerves (23,24). We have recently developed improved fabrication methods that enable production of CG scaffolds with uniform, equiaxed, polygonal pores of controlled size (16,26). The microstructural and mechanical properties of these scaffolds have previously been characterized (16,26–28), allowing a series of standardized and well defined microstructural environments to be presented to individual cells within the scaffold. Most significant for this investigation, the average pore size and the strut modulus (also overall scaffold modulus) can be varied independently of one another.

Manipulation of CG scaffold microstructural (pore size) and mechanical (scaffold Young's modulus) properties was used to address the questions of how cell migration is influenced by the surrounding microenvironment and what the critical microstructural cues are that affect migratory behavior within a physiologically relevant ECM analog. By quantifying 3D migratory behavior of NR6 mouse fibroblasts in CG scaffolds of varying pore size, we found that cell migration speed decreases with increasing pore size. Independent variation of scaffold strut modulus found a biphasic relationship between cell speed and strut modulus, and confirmed that the microstructural (pore size) dependence of cell migration is not due to deviations in scaffold strut flexural rigidity with changing pore size. Finally, more in-depth analysis of individual migration tracks revealed that an increased density of junction points between the scaffold struts is correlated with increased cell speed and changes in cell persistence. Our results also show that cell speed is significantly greater along the struts than at the strut junctions, regardless of pore size. Our findings, on the whole, establish the relevance of junctional microstructure in guiding and enhancing cell migration for both exploratory and design purposes.

MATERIALS AND METHODS

Cell culture

Cell migration assays were performed with NR6 mouse fibroblasts, a cell line derived from the Swiss 3T3 fibroblast line (29). Cells were maintained in MEM-α supplemented with 2 mM L-glutamine, 7.5% fetal bovine serum, 100 U/ml penicillin and 100 μg/ml streptomycin, 0.1 mM nonessential amino acids, and 1 mM sodium pyruvate (complete medium; all components from Invitrogen, Carlsbad, CA).

Collagen-GAG scaffold fabrication and cross-linking

CG scaffolds were fabricated from a suspension consisting of type I collagen (0.5 wt %) isolated from bovine tendon (Integra LifeSciences, Plainsboro, NJ) and chondroitin 6-sulfate (0.05 wt %) isolated from shark cartilage (Sigma-Aldrich, St. Louis, MO) in a solution of 0.05 M acetic acid (pH 3.2) via a lyophilization process described previously (16,24,26). In short, the aqueous suspension of precipitated collagen-GAG is solidified at a constant cooling rate from room temperature to a final freezing temperature, resulting in a continuous, interpenetrating network of ice crystals surrounded by the CG coprecipitate. Sublimation of the ice crystals produces the highly porous scaffold structure defined by individual fibers of CG, termed struts. Final freezing temperatures of -10, -20, -30, and -40°C were used to produce scaffolds of different mean pore size (96, 110, 121, and 151 μm, respectively (Table 1)). These scaffolds have previously been found to be microstructurally uniform, with equiaxed pores throughout the scaffold defined by struts of uniform thickness along their length (16,28). Finally, scaffolds were cross-linked using a dehydrothermal-based (DHT) process at 105°C for 24 h, as previously described (24), and cut into 6-mm-diameter disks. To vary scaffold

TABLE 1 Mean pore size, Young's modulus, and relative density of the DHT cross-linked CG scaffold variants, and motile fraction and cell speed for NR6 fibroblasts within the scaffold variants

T_f (°C)	Pore size (μm)	Scaffold elastic moduli (E^*) (Pa)	Relative density	Motile fraction	Cell speed (μm/h)
−10	151 ± 32	229 ± 22	0.0062 ± 0.0005	0.31	6.38 ± 0.50
−20	121 ± 23*	221 ± 47	0.0061 ± 0.0003	0.36	7.96 ± 0.52*
−30	110 ± 18**	176 ± 41	0.0059 ± 0.0003	0.41*	9.43 ± 0.53**
−40	96 ± 12***	206 ± 36	0.0058 ± 0.0003	0.69**	11.98 ± 0.61***

Elastic moduli and relative densities are taken from O'Brien et al. (16). Data are expressed as mean ± SD. *, **, and *** denote distinct, statistically significant results ($p < 0.05$).

strut modulus independently of pore size, we further cross-linked scaffold samples with a constant pore size (96 μm) with varying ratios of 1-ethyl-3-(3-dimethylaminopropyl)carbodiimide (EDAC) to N-hydroxysuccinimide (NHS) (Sigma-Aldrich) to collagen carboxylic acid groups (COOH) as previously described (25). A series of four DHT and EDAC cross-linking treatments were used: DHT 105°C for 24 h (DHT105/24), 1:1:5 EDAC/NHS/COOH ratio (EDAC1:1:5), 5:2:5 EDAC/NHS/COOH ratio (EDAC5:2:5), and 5:2:1 EDAC/NHS/COOH ratio (EDAC5:2:1). DHT and EDAC based cross-linking does not result in any microstructural (pore size) changes in the CG scaffold; due to the open cell nature of the scaffolds, cross-links are introduced within fibers (struts) rather than between fibers (23,30).

Thermal conditions during scaffold fabrication and cross-linking were chosen so as to not introduce any changes in scaffold surface chemistry, particularly collagen gelatinization, which results in significant structural changes to the collagen fibers (31–33). The CG scaffolds can be degraded by endogenously produced collagenase; in particular, fibroblasts have been identified as a major source of collagenase within in vivo wound sites (34). The in vivo and in vitro scaffold degradation rate can be modulated via cross-linking intensity (23); however, the in vitro degradation rates of the scaffolds used in this investigation are much slower (scaffold degradation half lives >1 month) than the timescale of this study (<1 day) (23,28,35,36), so changes in strut mechanical or microstructural properties due to cell-mediated degradation are not considered significant factors in this analysis.

Cellular solids modeling

The complex geometry of scaffolds is difficult to replicate exactly. We have previously used a tetrakaidecahedral unit cell (a fourteen-sided polyhedron) to model the geometry of the CG scaffolds (16,25,27,28,37). The tetrakaidecahedron packs to fill space and approximates the structural features of low-density foams observed through experiment (37). The dimensionless measure of total edge length per (unit volume)$^{1/3}$ for the tetrakaidecahedron is nearly identical to that observed for many random cellular structures (38), suggesting that it gives a good representation of the contact guidance cues (individual scaffold struts) provided by the CG scaffold. The tetrakaidecahedral cell has been successfully used to model CG scaffold specific surface area and permeability (16,27). For scaffolds with variable pore size (d) but constant relative density (ρ^*/ρ_s), the ratio of the scaffold strut thickness and length (l and t) can be described by Eq. 1 (37):

$$\frac{t_1}{l_1} = \frac{t_2}{l_2}, \tag{1}$$

where t_1 and l_1 are the thickness and length of the struts in scaffold 1 and t_2 and l_2 are those for scaffold 2. Note that the relative density of the scaffold is calculated from ρ^*, the density of the foam (CG scaffold), and ρ_s, the density of the solid strut material (bulk CG content), and can be calculated in terms of the mean length, l, and thickness, t, of the scaffold strut:

$$\frac{\rho^*}{\rho_s} = \frac{Vol_{solid}}{Vol_{foam}} \propto \frac{l \times t^2}{l^3} \propto \left(\frac{t}{l}\right)^2. \tag{2}$$

The CG scaffold pore microstructure is defined by an interconnected series of CG struts that meet at strut junctions. The spacing between (D_{jxn}) and density of strut junctions (ρ_{jxn}: number of strut junctions per unit cell divided by the volume of a unit cell) within the CG scaffold microstructure can be calculated from the scaffold pore size and tetrakaidecahedral unit cell model geometry:

$$D_{jxn} = l = \frac{d}{2.785} \tag{3}$$

$$\rho_{jxn} = \frac{6(jxns/UC)}{11.31 \cdot \left(\frac{d}{2.785}\right)^3 (vol/UC)} = \frac{11.459}{d^3}. \tag{4}$$

In the linear elastic regime, open-cell foams deform by strut bending. It is easily shown that the Young's modulus of the foam (or the scaffold), E^*, is given by (37):

$$E^* = C \times E_s \times \left(\frac{\rho^*}{\rho_s}\right)^2, \tag{5}$$

where E_S is the Young's modulus of the solid strut material, ρ^*/ρ_S, is the relative density, and C is a constant of proportionality related to the cell geometry; data for a wide variety of open-cell foams indicate that $C \approx 1$ (37). For open-cell foams such as the CG scaffold, E^* is independent of the pore size (37).

CG scaffold microstructural and mechanical properties

Mechanical and microstructural characterization of the CG scaffolds used in this investigation have been reported previously (16,25,26). Here we summarize the results of the previous characterization and how they apply to the current investigation. The relative density (ρ^*/ρ_s) and linear elastic modulus (E^*) of the CG scaffolds are presented in Tables 1 and 2; no effect of scaffold pore size (96–151 μm) on CG scaffold modulus (25) was observed. The hydrated modulus of the individual struts that make up the CG scaffold microstructure (E_s) was calculated to be 5.28 ± 0.25 MPa based on the measured dry strut modulus (E_s = 762 ± 35.4 MPa) and the relative difference in the dry and hydrated CG scaffold elastic modulus for the DHT (Standard) cross-linking ($E^*_{hydrated}/E^*_{dry} = 0.00693$) (25). This calculation was based upon the observed homogeneity of scaffold pore microstructure between the hydrated and dry phases, as well as previously verified cellular solids theory; a much more complete analysis, including the experimental assumptions and modeling employed to determine the CG scaffold microscale and macroscale mechanical properties has been published by these authors (25). The strut moduli for scaffolds cross-linked by the other techniques ($E_{s,other}$) were obtained via calculation (25):

$$E_{s,other} = E_{s,DHT} \times \frac{E^*_{other}}{E^*_{DHT}}, \tag{6}$$

where $E_{s,other}$ (unknown to be calculated) and $E_{s,DHT}$ (experimentally determined) are the strut moduli and E^*_{other} and E^*_{DHT} (experimentally determined) are the scaffold moduli (Tables 1 and 2) (25).

Fluorescent labeling of CG scaffolds

For multichannel imaging of fluorescent cells and scaffolds (Fig. 1 *A*), dry scaffold disks were fluorescently labeled by hydrating the scaffold with 5 μg/ml AlexaFluor 633 carboxylic acid, succinimidyl ester (Invitrogen) in phosphate-buffered saline (PBS) (Invitrogen) for 1 h at room temperature. Scaffolds were washed three times with PBS before seeding them with cells and imaging cells at 488-nm excitation, as described below, and AlexaFluor-633-labeled scaffolds at 647-nm excitation via confocal microscopy.

3D time-lapse confocal microscopy assay

NR6 fibroblasts were fluorescently labeled with 8 μM CellTracker Green CMFDA (Invitrogen) in complete medium for 20 min, washed twice with PBS, trypsinized, and resuspended in complete medium. We seeded 2.5×10^5 cells in 10 μl complete medium onto each side of an unlabeled scaffold disk prehydrated in complete medium to a final concentration of 5×10^5 cells/scaffold. Cells were allowed to attach to the scaffold in an ultra-low-attachment six-well plate (Corning, Corning, NY) for 1 h before the addition of complete medium and incubation for 12 h (39). Cell movement was imaged with a PerkinElmer RS-3 confocal microscope at 25× magnification and 488-nm excitation by collecting a 15-min interval time-lapse series of 100 μm z-stacks with 1-μm spacing over 10 h for a final field of view of $364 \times 246 \times 100$ μm. Care was taken to distinguish cell-mediated contraction from cell migration. Cell contraction within the CG scaffold is marked by buckling of the strut the cell is attached to and deformation of the surrounding scaffold microstructure (39,40). Previous investigation of cell contraction within the CG scaffold found that only a fraction of the cell population expresses a contractile phenotype, that those contractile cells are not motile during contraction, and that cell contraction and the associated scaffold deformation reach a steady state within 12 h of cell seeding (time constant 5.1 h) (28,39,40). The 12-h incubation time after seeding and before confocal imaging was chosen to allow nearly all cell contraction to occur. Further, when contractile cells were still active in the local environment of the region being imaged, image drift was observed where all or a significant number of cells within the field of view translocated together without displaying active movement. All experiments where drift was observed at any point were removed from analysis.

Single-cell tracking and quantitative analysis of cell migration

Centroids of fluorescent cells were computed with Imaris (Bitplane, St. Paul, MN) using the built-in ''spots'' function, and tracks of individual cells were generated with ''autoregressive motion'' tracking algorithms as described previously (Fig. 1 *B*) (6). Cells that migrate out of the field for more than 5 h as well as cells undergoing division or blebbing were ignored from further analysis. Nonmotile cells are defined as cells that do not display displacements more than the cell diameter, which has been measured to be ~10 μm, to avoid subjective categorization of nonmotile versus motile. Cells that moved more than 10 μm over 10 h were considered motile and their tracks were included in the quantitative analysis. Presented results were robust to the choice of the distance (data not shown). The proprietary Imaris spot-tracking algorithm used to determine cell centroid position has been previously validated for live-cell tracking (6); nevertheless, all cell tracks have been validated manually to eliminate all algorithm-generated errors. Three-dimensional wind-rose plots were generated by randomly choosing 40 tracks from the motile population and overlaying the starting coordinates at the origin of the plots to graphically represent average cell dispersion during migration. Average individual cell speeds (S) were calculated from individual cell tracks by averaging the distances over the time interval. This average cell speed calculation was taken for the entire cell track with no consideration made regarding the microstructural features of the scaffold. Mean-squared displacements (MSD) at various time intervals (t) were calculated using the method of nonoverlapping intervals (41) and directional persistence time (P) was obtained by fitting it to the persistent random walk (PRW) model:

$$MSD = 2S^2P[t - P(1 - e^{-t/P})]. \quad (7)$$

Cell speed data from $N > 3$ biological replicates was represented using box-and-whisker plots, where the edges of the boxes represent the 25th and 75th percentiles and the error bars represent the 10th and 90th percentiles. The line dividing the box represents the median, and the large dot represents the mean of the distribution. Statistical significance ($p < 0.05$) was determined via Students' t-test for motile fraction data and via Kolmogorov-Smirnov test for nonnormally distributed data sets, such as cell speed and persistence data.

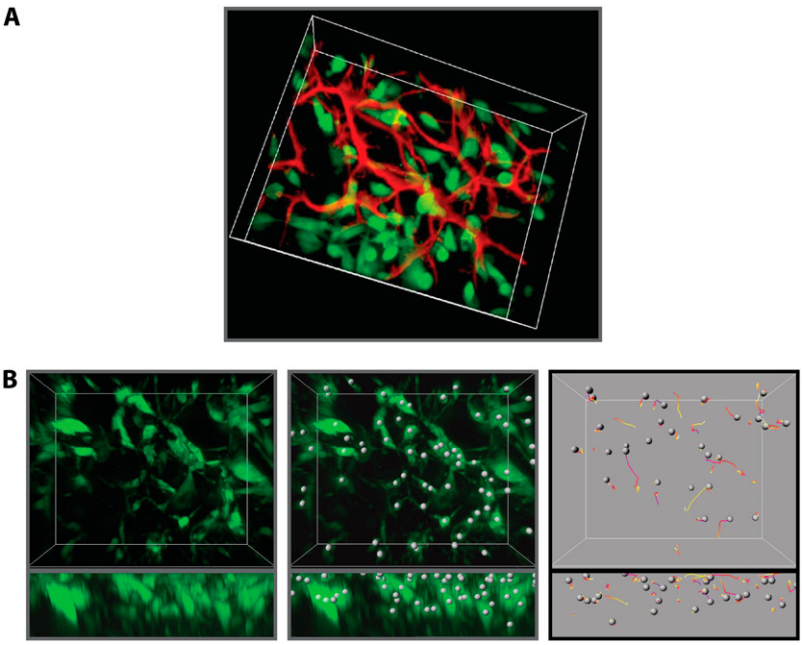

FIGURE 1 Sparsely seeded NR6 fibroblasts in a three-dimensional, highly porous CG scaffold. (*A*) Three-dimensional confocal micrograph of the porous microstructure of a CG scaffold (*red*) seeded with labeled NR6 cells (*green*). Note that the scaffold pore size is significantly larger than the dimension of an NR6 fibroblast. (*B*) *xy* and *xz* projections (*top* and *bottom boxes*, respectively) of individual cells tracked during migration in a CG scaffold. After capturing images via 3D time-lapse confocal microscopy (*left*), centroids of fluorescent NR6 cells are computed (*center*) and individual cell tracks generated (*right*). Cell tracks are color-mapped from blue to white indicating the beginning to the end of the movement. The mean pore size of CG scaffolds depicted is 96 μm and the 3D image dimensions are $364 \times 246 \times 100$ μm.

Cell turning time analysis

Cell tracks were independently analyzed for ''turning'' behavior, indicative of migration at a strut junction, versus ''straight'' migration behavior, indicative of migration along a strut. Consistently erratic movement over mostly relatively short distances was classified as turning behavior, whereas directional movement with relatively large distances (approximately greater than two cell lengths) was classified as straight motion. Time points that belong to turning behavior were quantified as ''time spent turning''. Each cell track was parsed into regions corresponding to straight migration versus turning migration behavior; the average migration speed of each motile cell while turning or migrating straight was calculated from these parsed tracks.

RESULTS

Cell migration in 3D CG scaffolds decreases as pore size increases

CG scaffolds exhibit pore sizes that are significantly larger than the characteristic dimension of NR6 fibroblasts (Fig. 1 *A*); hence, cells are not exposed to steric hindrance such as in a dense network of ECM fibers. Rather, cells are forced to migrate along scaffold struts, a phenomenon known as contact guidance. The NR6 fibroblasts displayed nonstraight line movement as they migrated through the CG scaffold network, including some back-and-forth movement. Final displacements (the difference between the starting and final coordinates of each cell) ranged from 10 μm to 78 μm; however, the total cell path length, which takes into account the back-and-forth motion exhibited by some cells, ranged as high as 180 μm for individual cells in our experiments.

To specifically address the question of how scaffold pore size affects cell migration behavior, we seeded NR6 mouse fibroblasts in CG scaffolds (DHT105/24) with pore sizes ranging from 96 μm to 151 μm and tracked single cell migration using 3D time-lapse confocal microscopy. A 10-h series of 3D volume stacks of fluorescently labeled cells in unlabeled scaffolds was generated, 3D coordinates of centroids of individual cells were determined over time, and individual tracks were generated (Fig. 1 *B*). Tracks from at least three biological replicates unexpectedly show that cells migrating in scaffolds with larger pore sizes exhibit less dispersion (Fig. 2 *A* (wind-rose plot)) and are less motile (Fig. 2 *B*) than cells migrating in scaffolds with smaller pores. Further quantification of these tracks shows that cell speed of the motile fraction significantly decreases with increasing scaffold pore size (Table 1 and Fig. 2 *C*); cell speed is reduced by nearly half, from ~12 μm/h to 6 μm/h, over the pore size range from 96 μm to 151 μm.

Changes in strut flexural rigidity are not responsible for dependence of cell speed on scaffold pore size

Previous studies of cell motility on 2D substrates (3) and within 3D gel constructs (6) show that substrate mechanical properties can strongly influence cell motility. We studied whether the observed influence of scaffold pore size on cell motility was due to differences in scaffold mechanical features with pore size. Specifically, mechanical and microstructural features of the individual scaffold strut was considered because cells migrating within the CG scaffolds likely obtain mechanical cues from the individual struts they are attached to rather than from the network of struts that defines the scaffold microstructure. The rationale for this is that there is no mechanism for a cell to ''feel'' the stiffness of

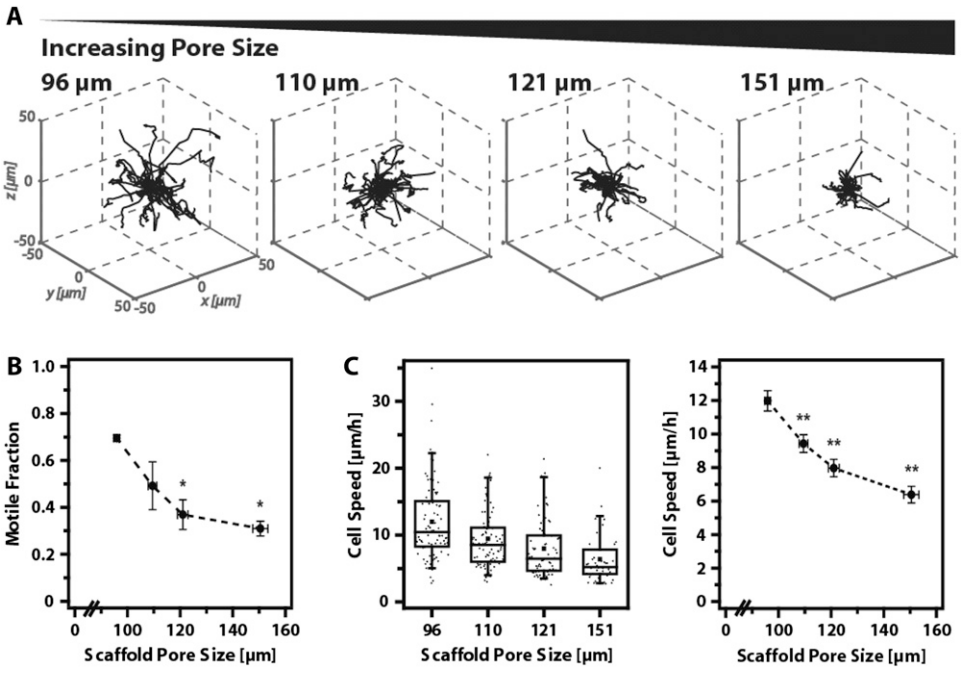

FIGURE 2 Cell migration behavior decreases with increasing mean scaffold pore size. Tracks of NR6 cells migrating in CG scaffolds with four distinct mean scaffold pore sizes (96–151 μm) were determined using 3D time-lapse confocal microscopy. (*A*) Three-dimensional wind-rose plots of randomly chosen cell tracks (40/condition) graphically represent the average cell dispersion from its starting point. Decreased dispersion is seen as scaffold mean pore size increases, from left to right. (*B*) Fraction of cells determined as motile (see Materials and Methods) from three biological samples were plotted against mean scaffold pore size. Total number of cells tracked, $N = 163$, 203, 229, and 131. (*C*) Box-and-whisker plot of cell speed of each individual cell determined as motile (Fig. 2 *B*). Mean and standard error of the dataset is plotted as a summary (*right*). From left to right, $N = 50$, 73, 94, and 90, respectively. Statistical significance (*, **: $p < 0.05$) is determined by pairwise Kolmogorov-Smirnov test for nonnormally distributed data sets.

the entire scaffold network; in scaffolds with pore sizes larger than the cell, the feature that a cell can attach to is an individual strut. Cells have been hypothesized and observed to probe their local mechanical environment by applying a load and measuring a displacement; a study of fibroblast contraction within this CG scaffold system has previously shown that for a range of system stiffnesses, cells apply a constant force, giving correspondingly different deformations (39,42). Due to their porous nature, the mechanical properties of the entire scaffold network are significantly different from the individual strut, and scale by a factor of the relative density squared (25,37). For example, for the CG scaffolds (0.6% relative density) with conventional DHT cross-linking, the elastic modulus of the individual strut ($E_S = 5.28$ MPa) is ~25,000 times greater than the scaffold network ($E^* = 208$ Pa) (25). Cellular solids models and experimental studies of strut buckling in open-cell foam systems has shown a negligible effect of the surrounding strut network on the buckling behavior of an individual strut (37): the end constraint factor for strut buckling does depend on the flexural rigidity of the adjacent strut, but assuming that the number of struts at each junction is, on average, comparable, it does not depend on the pore size or the relative density of the foam. Despite the large CG scaffold strut stiffness, the strut can be initially buckled by an applied load of 25 nN, due to the small dimensions of the strut, a level readily achievable by individual cells (28). The strut flexural rigidity, a measure of the ease with which a scaffold strut bends may be a more relevant biophysical parameter to consider for affecting cell behavior than the strut material modulus alone (43).

The flexural rigidity ($E_s \times I$) is defined by the elastic modulus (E_s) and the moment of inertia of the strut ($I = \pi \times t^4/64$), where t is the strut thickness. For the CG scaffolds with variable pore size (Table 1), the scaffold Young's modulus (E^*), strut Young's modulus (E_s), and scaffold relative density (ρ^*/ρ_S) are constant for all variants (25). However, scaffolds with increasing pore size have slightly longer ($l_{151\mu m} > l_{96\mu m}$) and thicker ($t_{151\mu m} > t_{96\mu m}$) struts (Eqs. 1 and 2, and Fig. 3 *A*). The strut moment of inertia (I) therefore increases with increasing pore size. The strut flexural rigidity of the scaffold with the largest pore size (151 μm) was calculated to be greater than the scaffold with the smallest pore size (96 μm) by a factor of 6.1 (data not shown).

The influence of scaffold pore size on cell motility might be explained by a mechanosensitive hypothesis where changes in strut flexural rigidity accounted for the differences in motility observed for cells in scaffolds with different pore sizes but constant strut modulus. However, an identical change in strut flexural rigidity can also be obtained by changing the strut modulus via cross-linking in a series of scaffolds with a constant pore size. To test the mechanosensitive hypothesis, we experimentally increased strut flexural rigidity by further cross-linking CG scaffolds of constant microstructure (pore size 96 μm) with EDAC, increasing strut elastic moduli by a factor of 7.2 across a range from 5.3 MPa to 38.0 MPa (Table 2). For the earlier portion of this study using different scaffold pore sizes, changes in strut flexural rigidity were wholly due to changes in strut moment of inertia ($E_s \times I$ increased by a factor of 6.1); for this portion of the study using variable cross-linking, changes in strut flexural rigidity were wholly due to changes in strut elastic modulus (increase by a factor of 7.2). In both cases, the reference scaffold (96-μm pore size, DHT cross-linking) was identical, so the relative increase in $E_s \times I$ (6.1-fold increase with changing pore size versus 7.2-fold increase by changing strut modulus) covered the same range. If local micromechanical influences, manifested through strut flexural rigidity, are responsible for the observed influence of scaffold pore size on cell motility, similar motile behavior of cells placed in scaffolds with variable strut moduli would be expected.

Migration of NR6 fibroblasts in the series of DHT- and EDAC-cross-linked scaffolds of constant pore size (96 μm) was tracked and the average cell speed was plotted against scaffold strut modulus (Table 2 and Fig. 3 *B*). The migration speed exhibited a subtle biphasic behavior with strut modulus, increasing significantly from 11 to 15 μm/h for strut moduli between 5 and 12 MPa, and then decreasing significantly back to 12 μm/h for strut moduli of 39 MPa. The expected decrease in cell speed with increasing strut elastic moduli according to the mechanosensitive hypothesis that considered strut flexural rigidity was not observed, suggesting that the effect of scaffold pore size on cell motility was not due to local changes in strut mechanical properties.

Cellular solids modeling and directional persistence analysis suggest a correlation between junction geometry and pore-size-dependent regulation of cell speed

Cellular solids analysis was further used to consider potential local contact guidance cues that may explain the influence of pore size on cell motility. CG scaffolds consist of struts that meet at strut junctions. The strut junction spacing (D_{jxn}) increases with increasing pore size (Eq. 3) and the strut junction density (ρ_{jxn}) decreases with increasing pore size (Eq. 4). Using these relationships, cell-speed data for scaffolds of varying pore size was replotted against junction spacing and junction density; the high degree of correlation (linear regression, $R^2 = 0.901$ and $R^2 = 0.998$, respectively) suggests that migratory behavior may be governed by the junction geometry of the scaffold (Fig. 4 *A*).

To test this novel hypothesis, we utilized the PRW model to determine persistence times for individual cell tracks within the scaffolds; the persistence times quantify the degree of directionally productive (''directional'' or ''straight'') rather than erratic (''turning'') cell locomotion (Fig. 4 *B*). Although the PRW model (Eq. 7) assumes a homogeneous, isotropic environment (i.e., a gel rather than a scaffold structure), we applied this model here only as a descriptive model in an attempt to correlate directionally productive

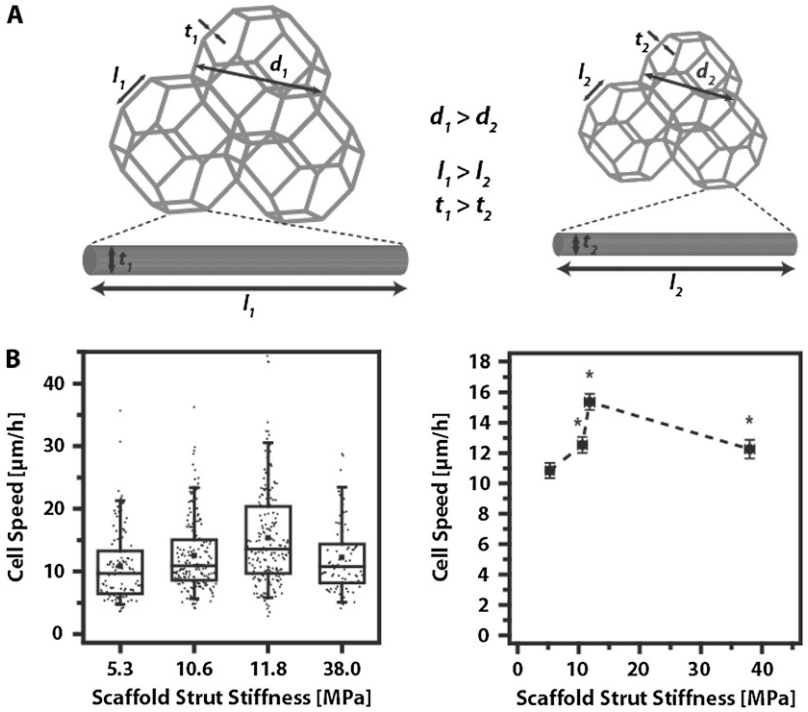

FIGURE 3 Subtle biphasic relationship is observed between cell migration speed and CG scaffold strut modulus; pore-size-dependent variation in cell speed is not explained by the variation in scaffold strut flexural rigidity. (*A*) Tetrakaidecahedral unit cell model for CG scaffold. For a series of scaffolds with a constant relative density, those with larger pore sizes, d_1 (*left*), exhibit struts that are longer and thicker than a scaffold with smaller pore sizes, d_2 (*right*). The longer/thicker struts have a greater flexural rigidity ($E_s \times I$) than the shorter/thinner struts, and would deform less under a constant cell-applied traction force. If changes in strut $E_s \times I$ explain the pore-size-dependent effect on cell motility, cell speed would be expected to decrease with increasing strut modulus. (*B*) Average speed of NR6 cells migrating in scaffolds with a constant microstructure (pore size 96 μm) but with varying strut modulus (over the same range as due to changes in strut $E_s \times I$) shown via box-and-whisker (*left*) and mean ± SE (*right*) plots. From left to right, $N = 116$, 188, 191, and 79, respectively. Distinct from the concept of decreasing cell speed with increasing modulus, as predicted if the pore-size-dependent effects on motility are due to changes in strut $E_s \times I$, a subtle biphasic relationship is seen between cell speed and substrate modulus. Statistical significance ($^*p < 0.005$) is determined by pairwise Kolmogorov-Smirnov test for nonnormally distributed data sets.

motion to cell migration along struts. Hence, persistence time as defined here describes not the cell's intrinsic persistence, but directionally productive motion as influenced by the extracellular environment. Cells migrating in scaffolds with larger pore sizes exhibit greater persistence times, indicating more directional motion. In contrast, persistence times of cells migrating in scaffolds with smaller pore sizes and greater junction density are significantly lower.

Analysis of turning movement confirms that increased cell speed is linked with movement at strut junctions

In an attempt to further correlate cell speed and localization of cells in the scaffold, each cell locomotion path was analyzed in detail by assigning local migration behavior to turning or directional movement categories. Turning movement is correlated to migration at strut junctions and directional movement to migration along struts (see Materials and Methods). Only a small fraction of cells were able to ''jump'' from one strut to another (data not shown), validating our binary characterization. The time periods for each individual cell track in these two categories were quantified and normalized to the total track time for each cell path, enabling an overall population-averaged plot of the fraction of total time spent turning by cells within each scaffold variant (Fig. 4 *C*). This analysis shows that cells spend almost 50% of their time turning in the smallest pore size scaffold (that with the largest ρ_{jxn}), and that the proportion of their movement time devoted to turning decreases steadily and substantively as scaffold pore size increases (decreasing ρ_{jxn}). In the largest pore size, cells migrate with only 20% of their time spent turning and, consequently, 80% of their time spent continuing directional movement. Further analysis of cell locomotion during turning versus directional movement showed that cell migration speed along struts (Fig. 5 *A*) or at strut junctions (Fig. 5 *B*) decreases with increasing pore size. It is of interest to note that the migration speed along the struts in the 151-μm scaffolds is less than half that for the 96-μm scaffolds. Cell migration speed is significantly faster along the struts (''straight'' speed) than at strut junctions (''turning'' speed) in each scaffold regardless of pore size (Fig. 5 *C*). These results suggest a potential mechanistic explanation for our initially counterintuitive observation that cell motility de-

TABLE 2 Scaffold and strut elastic moduli, motile fraction, and cell speed in cross-linked scaffold variants of NR6 fibroblasts

Cross-linking treatment	Scaffold elastic moduli (E^*) (Pa)	Scaffold strut elastic moduli (E_s) (MPa)	Motile fraction	Cell speed (μm/h)
DHT (standard)	206 ± 36	5.28 ± 0.25	0.69	10.84 ± 0.54
EDAC1:1:5	225 ± 11	10.6 ± 0.50*	0.75	12.53 ± 0.42*
EDAC5:2:5	410 ± 30*	11.8 ± 0.56**	0.86	15.35 ± 0.56**
EDAC5:2:1	1480 ± 210**	38.0 ± 1.8***	0.77	12.25 ± 0.64*

Cross-linking techniques have been described by Harley et al. (25). Data are expressed as mean ± SD. *, **, and *** denote distinct, statistically significant results ($p < 0.05$).

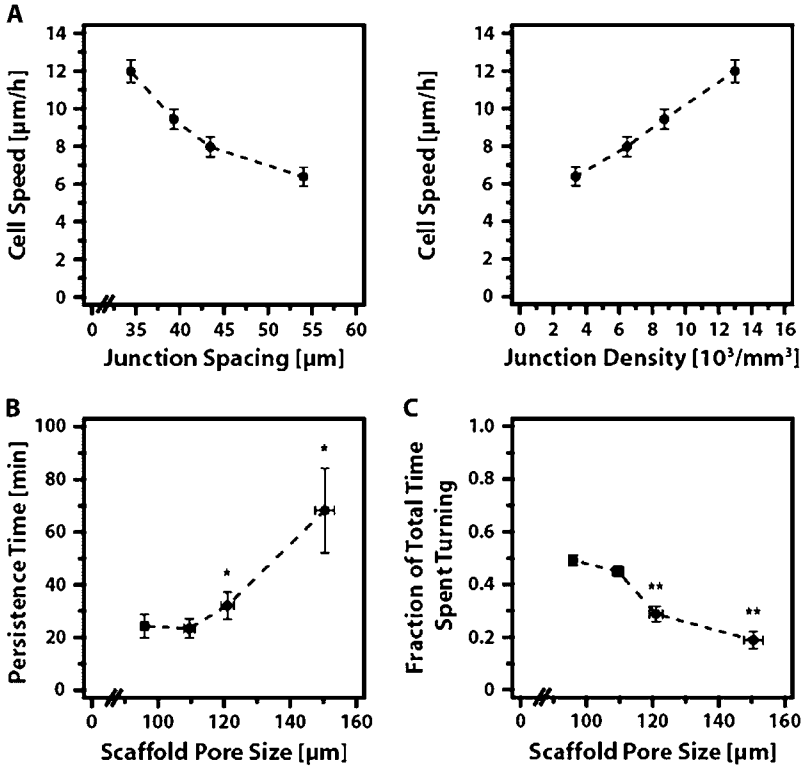

FIGURE 4 Cell migration appears to be influenced by strut junctions within the scaffold microstructure. (*A*) Cell speed is replotted against junction spacing (*left*) and junction density (*right*), pore-size-dependent parameters calculated from the tetrakaidecahedral unit cell model. (*B*) Persistence times of individual cells migrating in scaffolds of varying pore size were calculated from the PRW model; for scaffolds with decreasing strut junction density (increasing distance between strut junctions), cells were observed to have increasing persistence times. (C) Cell turning was categorized as short, erratic movement and is indicative of migration at junctions. The time spent turning, as opposed to moving directionally, was determined for each distinct cell track and normalized against the total time spent migrating. The fraction of time the cell spent turning was observed to significantly decrease with increasing pore size (decreasing strut junction density, increasing distance between strut junctions). All data are shown as mean ± SE. Statistical significance (*: $p < 0.05$; **: $p < 0.02$) is determined by pairwise Kolmogorov-Smirnov test for non-normally distributed data sets.

creases as scaffold pore size increases (Fig. 2). These results suggest new hypotheses, as well as future experiments for testing these hypotheses, described in the next section.

DISCUSSION

CG scaffolds have found useful application as ECM analogs for regeneration of a variety of tissue types (23,24,34). Here, we took advantage of the uniform pore microstructure of these standardized, well characterized CG scaffolds along with the ability to independently vary their pore size and strut modulus to assess how these parameters affect cell motility. Through a comprehensive, quantitative analysis of individual migration tracks of fibroblasts, we observed that NR6 fibroblast migration was significantly influenced by the scaffold pore size and scaffold strut modulus (Figs. 2 and 3). The subtle biphasic dependence of scaffold strut modulus (E_s) on cell migration speed (Fig. 3) correlates well with previous experimental and computational studies of cell motility in dense 3D materials with a high degree of steric hindrances (6,7). However, the strong dependence of cell migration on pore size was not expected, since the porous CG scaffolds do not present steric hindrances. The role of strut flexural rigidity in influencing cell motility was tested and discounted as a mechanism for explaining the influence of scaffold pore size on cell motility (Fig. 3).

A quantitative, theoretical analysis using cellular solids modeling revealed that decreasing mean scaffold pore size leads to an increase in the number of strut junctions, which are points in the scaffold microstructure where two or more struts meet. Strut junctions are discrete areas of significantly different extracellular morphology compared to an individual strut. With the average strut length of the order of 30–60 μm for the different scaffolds used in this investigation, motile cells as well as sessile cells extending processes along individual struts are expected to—and have been observed to—regularly encounter multiple strut junctions during the 10-h imaging period of this experiment. If cell motility were influenced by strut junctions, it is potentially the change in the extracellular morphology and mechanics at the junctions that is responsible for this effect.

We therefore examined the possibility that cell migration behavior at strut junctions may be significantly different from that along the struts. Multiple struts branching out in 3D allow cells to probe multiple paths before following a single path for migration. Fibroblast lamellipodia at the leading edge of the migrating cell are known to extend directed, local protrusions as well as synchronous transverse protrusions that probe for new adhesion sites and direct migration, playing a central role in path-finding and mechanotransduction during motility (44,45); transverse lamellipodial protrusions may be especially significant here when considering strut junctions, as they allow the cell to navigate the strut junction complex by sampling more of the surrounding scaffold microstructure through its cell surface adhesion receptors than can be achieved with simple forward and backward probing. Such probing movements at the junctions are likely characterized by the erratic ''turning'' movement of the entire cell observed experimentally.

Unfortunately, we found that direct, simultaneous visualization of cells and scaffold with confocal microscopy for

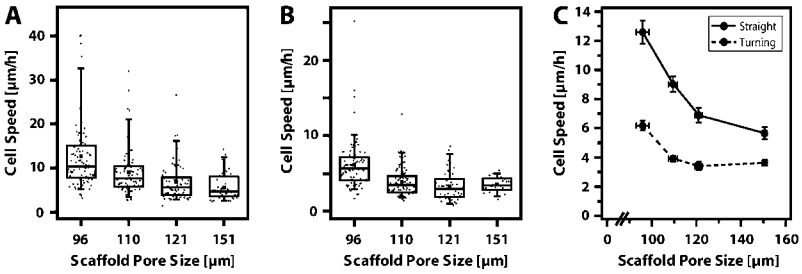

FIGURE 5 Cell migration speed is significantly influenced by the presence of strut junctions. Average migration speed was determined within each cell track for the periods of time the cell spent (*A*) migrating directionally (''straight'', migrating along the strut) versus (*B*) migrating erratically (''turning'', migrating at strut junctions). A pore-size-dependent effect is observed on cells migrating along the struts or at the junctions; cells are observed to migrate more slowly as pore size increases (strut junction density decreases, distance between junctions increases). (*C*) Summarized mean ± SE plot of *A* and *B*. Regardless of scaffold pore size, cell migration speed is significantly faster along the struts than at strut junctions, suggesting that strut junctions play a key role in regulating cell motility through 3D, fibrillar ECM structures.

purposes of correlating a cell's speed and behavior with its location on the scaffold was not possible. Specifically, fluorescent labeling of the scaffold may alter the ligand distribution on the scaffold surface, and long-term two-channel image acquisition generated significant cell phototoxicity. Hence, indirect measures of scaffold localization were used to infer geographical information about the cells. Persistence times for individual cell movement (Fig. 4 *B*) indicated that cell migration in scaffolds with lower junction density (larger pore size) exhibited greater persistence times with more directional motion (correlative to migration along individual struts). On the other hand, persistence times of cells migrating in scaffolds with greater junction densities (smaller pore size) were indicative of erratic movement, likely occurring more often at junctions that have the potential for cells to adhere to multiple struts (Fig. 4 *B*). To support these findings, each cell locomotion path was analyzed and categorized as erratic turning movement, corresponding to movement at strut junctions, or directional movement, corresponding to movement along struts (Fig. 4 *C*). Indeed, cells migrating in scaffolds with higher junction density spent more time turning at strut junctions than those migrating in scaffolds with lower junction density. These findings led to the speculation that strut junction geometry is responsible for the initially nonintuitive increase in speed of cells migrating in scaffolds with smaller pore sizes.

Results that cells exhibit enhanced motility due to scaffold junctions were counterintuitive at first, since the cells are given an opportunity to be ''indecisive'' at junctions, usually leading to a reduction in net locomotion, whereas struts only provide two opposite directions to migrate, raising the probability of exhibiting high cell locomotion. Previous in vivo contact guidance studies have shown cells migrating along single ECM fibers through a dense ECM network at high speeds up to 3 μm/min (12,46). However, these in vivo ECM fibers are much thicker than the struts in the CG scaffolds used here (of the order 3–5 μm), and due to the surrounding dense ECM structure in vivo, those cells were exposed to a significantly greater surface area (increased ligand exposure). It is well known that migration behavior is governed by ligand density and the ability to form ligand-receptor interactions on 2D substrata (47–49) and in 3D ECM gels (6). A single strut of our scaffold, providing almost a one-dimensional line to the cell, may not supply sufficient ligand density for movement with enhanced migration speed. However, strut junctions that present increased local ligand density may provide the necessary adhesion sites for increased migratory speed. In combination, multiple struts with options for movement in several directions may lead to a more erratic movement, but not to a reduction in cell speed, which was shown by our data (Figs. 4, *B* and C, and 5). There are no previous studies establishing relationships between dimensionality and cell speed, but this study may indicate that in the absence of steric hindrance (i.e., $n < 3$), an increase in dimensionality could lead to an increase in migration response.

Nevertheless, when interpreting these findings, it is to be noted that the average cell speed for motile cells was calculated as an average over the entire 10-h migration period; therefore, cell speed incorporates continuous, directional migration (along the struts), as well as turning behavior at the strut junctions. The influence of strut junction on cell speed likely manifests itself in one of two ways: increasing the migration speed along the struts between the junctions, or increasing the speed of the cell movements at the strut junctions. One could hypothesize that cells move at a constant rate along the struts but more rapidly at the strut junctions because they are attaching to several struts at once and therefore the cell is shifting rapidly over small distances (44). Because cells spend a greater fraction of time turning (at the junctions) in scaffolds with smaller pore sizes, rapid movement at strut junctions could be responsible for the increased overall average cell speed. However, if this were the case, cells in the smaller pore-size scaffold with the greatest strut junction density would also show decreased dispersion in the windrose plot due to the decreased time of directional movement, but in fact, the opposite is the case (Fig. 2 *A*). Therefore, strut junctions rather appear to increase cell motility by increasing the cell speed between junctions along the struts. Further analysis of the motility of cells along the struts at strut junctions confirmed this hypothesis (Fig. 5); although cells in scaffolds with increased junction densities had an increased

migration speed during turning, they showed a significantly greater increase in migration speed along the struts during directional motion. These results suggest that strut junctions play a central role in regulating cell motility in 3D scaffolds.

The relationship between scaffold microstructure and ligand presentation is an important relationship to consider in analyzing these results. Ligand density in the CG scaffold is a constant defined by the chemical composition. The role that strut junctions are hypothesized to play here in affecting motility is that the junction provides a different geometrical distribution of ligands available to the cell, as well as a different local mechanical environment. Local ligand availability at a strut junction is governed by the total surface area of struts that the cells are attaching to along with the spatial organization of the struts that define the junction. Further, since a junction is defined by multiple struts meeting at a single point, the local mechanical properties of the junction versus the individual strut are necessarily different. Therefore, it is possible that, in addition to changes in ligand density at strut junctions, cell motility is modulated by other factors. It is hypothesized that the mechanism for this modulation in cell motility involves local micromechanical differences, as well as cytoskeletal reorganization at the strut junctions due to differences between the strut and the strut junction in the local scaffold microstructure, which are affected by strut surface area and ligand density. Determining the role that ligands and the change in the local mechanical environment play in modulating cell behavior at the strut junctions versus along the strut are part of future planned experiments by these authors to continue to investigate how the local scaffold microenvironment can be manipulated to modulate cell behavior. Recent advances in imaging technology such as multiphoton microscopy, higher-resolution confocal microscopy, and (fluorescent) labeling techniques should prove invaluable to such future studies. The role of this article is to propose that strut junctions are a critical feature of porous biomaterials that needs to be considered when examining extracellular cues for cell behavior.

The ability to vary the scaffold and strut modulus independent of other scaffold properties through chemical cross-linking allowed us to rule out that the pore-size-dependent decrease in cell migration speed seen in Fig. 2 may be due to pore-size-dependent changes in the scaffold mechanical properties (strut flexural rigidity). En route, we were able to identify that individual cell migration behavior is biphasically dependent on strut elastic modulus (E_s, Fig. 3 *B*). Such biphasic dependence on substrate rigidity has been previously reported only in isotropic, homogeneous 2D and 3D network systems (6,7,18). These experiments looking at the effect of changes in scaffold strut modulus on cell motility, independent of microstructure (Fig. 3 *B*), were performed using scaffolds with the highest junction density (pore size 96 μm). Whether the biphasic dependence on stiffness would hold if scaffold modulus was varied in scaffolds of lower junction density is yet to be investigated.

Although we report a biphasic relationship between cell migration speed and scaffold strut modulus (E_s), when contemplating cell mechanosensing mechanisms in a porous biomaterial, a more detailed descriptor of the local microenvironment may be required. Details of such mechanosensing mechanisms are currently being studied (43), but a physiological readout of substrate compliance or stiffness is likely through the cell's ability to sense the deformation of its underlying substrate in response to a constant applied traction force. Dermal fibroblasts, as well as a number of other cell types, have been observed to contract CG scaffolds, significantly deforming the macroscopic shape of scaffold samples, as well as buckling the individual scaffold struts to which they are attached (28,39,50). Significantly, dermal fibroblasts are observed to apply a constant average contractile force per cell independent of the scaffold system stiffness (42), suggesting that the cell may sense underlying substrate stiffness or compliance through its deformation; these results suggest that strut flexural rigidity is the more appropriate variable to consider when describing scaffold mechanical properties and considering cell behavior.

The modulus of the CG scaffold struts (E_s) that the fibroblasts were migrating along ranged between 5.28 ± 0.25 and 38.0 ± 1.8 MPa (25). This range of moduli can be placed along a continuum that spans six orders of magnitude and that includes biologically derived and relevant materials used to study cell behavior, as well as natural tissues and ECM proteins. Elastic moduli for natural ECM in tissues range from 10 kPa for soft brain tissue to 20 GPa for cortical bone (20,51,52); however, as tissues are made up of a network of extracellular proteins and inorganic components, it is the mechanical properties of the individual fibrillar proteins within the tissue, to which individual cells attach, that are most important to consider. Significantly stiffer than the CG scaffold struts are many cytoskeletal and extracellular proteins such as actin (2.3 GPa), pure collagen fibrils (2 GPa), and tubulin (1.9 GPa), whereas keratin exhibits a modulus (2 MPa) closer to the CG strut modulus; however, proteolytic degradation of these proteins can significantly reduce their stiffness. Stiffer still are materials used for conventional studies of cell behavior on flat substrates such as tissue culture plastic (3.5 GPa) and glass (50 GPa). Although the CG scaffold struts exhibit elastic moduli in the range of 5–38 MPa, their dimensions are such that applied forces as low as 25 nN (28) can buckle an individual strut, making it possible for individual cells to actively sense their local mechanical microenvironment within the CG scaffold.

A potential confounding factor of the influence of different cross-linking treatments on CG scaffold strut ligand density was considered and discounted. DHT- and EDAC-based cross-linking have previously been shown to not introduce microstructural (pore-size) changes in the collagen-GAG scaffold structure; cross-links are introduced within fibers (struts) rather than between fibers, resulting in changes to the scaffold mechanical properties but not to microstructural

properties (23,30). Cross-linking entails activated carboxylic acid groups present on the polypeptide chains of collagen reacting with free amine groups on other peptide chains; previous investigation has found that amine groups on two adjacent fiber bundles (similar in dimensions to struts) were too far apart to be bridged by cross-links unless the fibers were specifically aligned (30), suggesting that cross-linking occurs within and not between the scaffold struts. Over the range of cross-linking treatments used (comparing noncross-linked collagen to the range of cross-linking treatments, notably from DHT105/24 to EDAC/NHS/COOH 5:2:1), the free amine groups present within the scaffold are reduced by $<$21 amines/1000 amino acid residues within the scaffold (30,32,33). Such a relatively small change in chemical composition, combined with the requirement for very close interaction between collagen fibrils for successful cross-linking, suggests that limited modification to the surface chemistry of each scaffold strut is expected; further, the wide range of available ligands and their associated chemical composition within the CG scaffold (53) suggest that EDAC and DHT cross-linking likely result in minimal changes to the overall ligand availability for cell attachment and migration. Still further, no qualitative differences in the overall shape or spreading behavior of individual cells was observed across the different scaffolds; future experiments will attempt to better evaluate such differences through examination of the size and distribution of focal adhesions on individual cells within each scaffold variant. However, the issue of small changes in the local scaffold chemical composition due to cross-linking and how this may affect cell behavior raises an important question for rigorous, future research.

The results of our study complement findings from previous studies that cell migratory behavior is nontrivially affected by multiple parameters and properties of the ECM (6,7). Our study not only highlighted the complex dependence of cell motility on matrix modulus in a highly porous ECM system consisting of struts and junctions, but also demonstrated the previously unexplored importance of the ECM microstructure in governing cell migration behavior. These findings were made possible by the ability to independently vary the mechanical and microstructural properties of the CG scaffolds. These scaffolds, comprised of naturally derived ECM components, serve as highly tunable substrates for porous and fibrous ECM systems that are relevant to tissue engineering applications and physiology. Other substrates, such as tissue samples or naturally derived in vitro ECM gels are less well suited for establishing a quantitative relationship between migratory behavior and parameters of the 3D ECM microstructure due to their complex and unpredictable microstructure. Other synthetic biomaterials (54) may allow subtle architectural control, but independent parsing of mechanical and geometrical properties has not yet been described. Our findings have implications for the design of tissue engineering substrates that require extensive migratory behavior; for example, a scaffold with an engineered higher strut junction density may accelerate cell in-growth into the initially acellular structure, a critical requirement for the development of large, porous implants for regenerative medicine applications. In addition, the specific influence of construct parameters such as chemical composition and degradation characteristics, along with the influence of environmental factors such as soluble regulator content (i.e., growth factor, cytokine), cell culture conditions, and exogenous loading, is unknown. Future studies may examine the application of the CG scaffold system described here to such areas.

The authors thank Prof. Paul Matsudaira for stimulating discussions and the Whitehead-MIT BioImaging Center for technical support.

We gratefully acknowledge support from the National Institute of General Medical Sciences Cell Migration Consortium NIH U54-GM064346 (H.D.K., M.H.Z., and D.A.L.), the Cambridge-MIT Institute (B.A.H., I.V.Y., and L.J.G.), the Matoula S. Salapatas Professorship in the Department of Materials Science and Engineering at MIT (L.J.G.), the Whitaker-MIT Health Science Fund Fellowship (B.A.H.), and the Sokol Foundation (M.H.Z.).

REFERENCES

1. Lauffenburger, D. A., and A. F. Horwitz. 1996. Cell migration: a physically integrated molecular process. *Cell*. 84:359–369.
2. Friedl, P., K. S. Zanker, and E. B. Brocker. 1998. Cell migration strategies in 3-D extracellular matrix: differences in morphology, cell matrix interactions, and integrin function. *Microsc. Res. Tech.* 43:369–378.
3. Lo, C. M., H. B. Wang, M. Dembo, and Y. L. Wang. 2000. Cell movement is guided by the rigidity of the substrate. *Biophys. J.* 79:144–152.
4. Munevar, S., Y. L. Wang, and M. Dembo. 2001. Distinct roles of frontal and rear cell-substrate adhesions in fibroblast migration. *Mol. Biol. Cell*. 12:3947–3954.
5. Wang, H. B., M. Dembo, S. K. Hanks, and Y. Wang. 2001. Focal adhesion kinase is involved in mechanosensing during fibroblast migration. *Proc. Natl. Acad. Sci. USA*. 98:11295–11300.
6. Zaman, M. H., L. M. Trapani, A. L. Sieminski, D. Mackellar, H. Gong, R. D. Kamm, A. Wells, D. A. Lauffenburger, and P. Matsudaira. 2006. Migration of tumor cells in 3D matrices is governed by matrix stiffness along with cell-matrix adhesion and proteolysis. *Proc. Natl. Acad. Sci. USA*. 103:10889–10894.
7. Zaman, M. H., R. D. Kamm, P. Matsudaira, and D. A. Lauffenburger. 2005. Computational model for cell migration in three-dimensional matrices. *Biophys. J.* 89:1389–1397.
8. Wolf, K., I. Mazo, H. Leung, K. Engelke, U. H. von Andrian, E. I. Deryugina, A. Y. Strongin, E. B. Brocker, and P. Friedl. 2003. Compensation mechanism in tumor cell migration: mesenchymal-amoeboid transition after blocking of pericellular proteolysis. *J. Cell Biol.* 160:267–277.
9. Zaman, M. H., P. Matsudaira, and D. A. Lauffenburger. 2007. Understanding effects of matrix protease and matrix organization on directional persistence and translational speed in three-dimensional cell migration. *Ann. Biomed. Eng.* 35:91–100.
10. Brock, A., E. Chang, C. C. Ho, P. LeDuc, X. Jiang, G. M. Whitesides, and D. E. Ingber. 2003. Geometric determinants of directional cell motility revealed using microcontact printing. *Langmuir*. 19:1611–1617.
11. Lehnert, D., B. Wehrle-Haller, C. David, U. Weiland, C. Ballestrem, B. A. Imhof, and M. Bastmeyer. 2004. Cell behaviour on micropatterned substrata: limits of extracellular matrix geometry for spreading and adhesion. *J. Cell Sci.* 117:41–52.
12. Condeelis, J., and J. E. Segall. 2003. Intravital imaging of cell movement in tumours. *Nat. Rev. Cancer*. 3:921–930.
13. Bajenoff, M., J. G. Egen, L. Y. Koo, J. P. Laugier, F. Brau, N. Glaichenhaus, and R. N. Germain. 2006. Stromal cell networks

regulate lymphocyte entry, migration, and territoriality in lymph nodes. *Immunity*. 25:989–1001.

14. Stachowiak, A. N., and D. J. Irvine. 2008. Inverse opal hydrogel-collagen composite scaffolds as a supportive microenvironment for immune cell migration. *J. Biomed. Mater. Res. A*. 85:815–828.
15. Nehrer, S., H. A. Breinan, A. Ramappa, G. Young, S. Shortkroff, L. K. Louie, C. B. Sledge, I. V. Yannas, and M. Spector. 1997. Matrix collagen type and pore size influence behaviour of seeded canine chondrocytes. *Biomaterials*. 18:769–776.
16. O'Brien, F. J., B. A. Harley, I. V. Yannas, and L. J. Gibson. 2005. The effect of pore size on cell adhesion in collagen-GAG scaffolds. *Biomaterials*. 26:433–441.
17. Wake, M. C., C. W. Patrick, Jr., and A. G. Mikos. 1994. Pore morphology effects on the fibrovascular tissue growth in porous polymer substrates. *Cell Transplant*. 3:339–343.
18. Peyton, S. R., and A. J. Putnam. 2005. Extracellular matrix rigidity governs smooth muscle cell motility in a biphasic fashion. *J. Cell. Physiol*. 204:198–209.
19. Grinnell, F., C. H. Ho, Y. C. Lin, and G. Skuta. 1999. Differences in the regulation of fibroblast contraction of floating versus stressed collagen matrices. *J. Biol. Chem*. 274:918–923.
20. Engler, A. J., S. Sen, H. L. Sweeney, and D. E. Discher. 2006. Matrix elasticity directs stem cell lineage specification. *Cell*. 126:677–689.
21. Yeung, T., P. C. Georges, L. A. Flanagan, B. Marg, M. Ortiz, M. Funaki, N. Zahir, W. Ming, V. Weaver, and P. A. Janmey. 2005. Effects of substrate stiffness on cell morphology, cytoskeletal structure, and adhesion. *Cell Motil. Cytoskeleton*. 60:24–34.
22. Capito, R. M., and M. Spector. 2003. Scaffold-based articular cartilage repair. *IEEE Eng. Med. Biol. Mag*. 22:42–50.
23. Harley, B. A., M. H. Spilker, J. W. Wu, K. Asano, H. P. Hsu, M. Spector, and I. V. Yannas. 2004. Optimal degradation rate for collagen chambers used for regeneration of peripheral nerves over long gaps. *Cells Tissues Organs*. 176:153–165.
24. Yannas, I. V., E. Lee, D. P. Orgill, E. M. Skrabut, and G. F. Murphy. 1989. Synthesis and characterization of a model extracellular matrix that induces partial regeneration of adult mammalian skin. *Proc. Natl. Acad. Sci. USA*. 86:933–937.
25. Harley, B. A., J. H. Leung, E. C. C. M. Silva, and L. J. Gibson. 2007. Mechanical characterization of collagen-GAG scaffolds. *Acta Biomater*. 3:463–474.
26. O'Brien, F. J., B. A. Harley, I. V. Yannas, and L. Gibson. 2004. Influence of freezing rate on pore structure in freeze-dried collagen-GAG scaffolds. *Biomaterials*. 25:1077–1086.
27. O'Brien, F. J., B. A. Harley, M. A. Waller, I. V. Yannas, L. J. Gibson, and P. J. Prendergast. 2007. The effect of pore size on permeability and cell attachment in collagen scaffolds for tissue engineering. *Technol. Health Care*. 15:3–17.
28. Harley, B. A., T. M. Freyman, M. Q. Wong, and L. J. Gibson. 2007. A new technique for calculating individual dermal fibroblast contractile forces generated within collagen-GAG scaffolds. *Biophys. J*. 93: 2911–2922.
29. Pruss, R. M., and H. R. Herschman. 1977. Variants of 3T3 cells lacking mitogenic response to epidermal growth factor. *Proc. Natl. Acad. Sci. USA*. 74:3918–3921.
30. Olde Damink, L. H. H., P. J. Dijkstra, M. J. A. van Luyn, P. B. Van Wachem, P. Nieuwenhuis, and J. Feijen. 1996. Cross-linking of dermal sheep collagen using a water soluble carbodiimide. *Biomaterials*. 17: 765–773.
31. Yannas, I. V., and A. V. Tobolsky. 1967. Cross linking of gelatine by dehydration. *Nature*. 215:509–510.
32. Sung, N. H. 1972. Structure and properties of collagen and gelatin in the hydrated and anhydrous solid state. Sc.D. thesis. Massachusetts Institute of Technology, Cambridge, MA.
33. Yannas, I. V. 1972. Collagen and gelatin in the solid state. *J. Macromol. Sci. Rev. Macromol. Chem*. C7:49–104.
34. Yannas, I. V. 2001. Tissue and Organ Regeneration in Adults. Springer, New York.
35. Yannas, I. V., J. F. Burke, C. Huang, and P. L. Gordon. 1975. Correlation of in vivo collagen degradation rate with in vitro measurements. *J. Biomed. Mater. Res*. 9:623–628.
36. Pek, Y. S., M. Spector, I. V. Yannas, and L. J. Gibson. 2004. Degradation of a collagen-chondroitin-6-sulfate matrix by collagenase and by chondroitinase. *Biomaterials*. 25:473–482.
37. Gibson, L. J., and M. F. Ashby. 1997. Cellular Solids: Structure and Properties. Cambridge University Press, Cambridge, UK.
38. Kraynik, A. M., D. A. Reinelt, and F. van Swol. 2003. Structure of random monodisperse foam. *Phys. Rev*. 67:031403.
39. Freyman, T. M., I. V. Yannas, R. Yokoo, and L. J. Gibson. 2001. Fibroblast contraction of a collagen-GAG matrix. *Biomaterials*. 22:2883–2891.
40. Freyman, T. M., I. V. Yannas, Y.-S. Pek, R. Yokoo, and L. J. Gibson. 2001. Micromechanics of fibroblast contraction of a collagen-GAG matrix. *Exp. Cell Res*. 269:140–153.
41. Dickinson, R. B., and R. T. Tranquillo. 1993. Optimal estimation of cell-movement indexes from the statistical analysis of cell tracking data. *AIChE J*. 39:1995–2010.
42. Freyman, T. M., I. V. Yannas, R. Yokoo, and L. J. Gibson. 2002. Fibroblast contractile force is independent of the stiffness which resists the contraction. *Exp. Cell Res*. 272:153–162.
43. Vogel, V., and M. Sheetz. 2006. Local force and geometry sensing regulate cell functions. *Nat. Rev. Mol. Cell Biol*. 7:265–275.
44. Galbraith, C. G., K. M. Yamada, and J. A. Galbraith. 2007. Polymerizing actin fibers position integrins primed to probe for adhesion sites. *Science*. 315:992–995.
45. Suter, D. M., and P. Forscher. 2001. Transmission of growth cone traction force through apCAM-cytoskeletal linkages is regulated by Src family tyrosine kinase activity. *J. Cell Biol*. 155:427–438.
46. Sidani, M., J. Wyckoff, C. Xue, J. E. Segall, and J. Condeelis. 2006. Probing the microenvironment of mammary tumors using multiphoton microscopy. *J. Mammary Gland Biol. Neoplasia*. 11:151–163.
47. DiMilla, P. A., K. Barbee, and D. A. Lauffenburger. 1991. Mathematical model for the effects of adhesion and mechanics on cell migration speed. *Biophys. J*. 60:15–37.
48. Huttenlocher, A., M. H. Ginsberg, and A. F. Horwitz. 1996. Modulation of cell migration by integrin-mediated cytoskeletal linkages and ligand-binding affinity. *J. Cell Biol*. 134:1551–1562.
49. Palecek, S. P., J. C. Loftus, M. H. Ginsberg, D. A. Lauffenburger, and A. F. Horwitz. 1997. Integrin-ligand binding properties govern cell migration speed through cell-substratum adhesiveness. *Nature*. 385: 537–540.
50. Torres, D. S., T. M. Freyman, I. V. Yannas, and M. Spector. 2000. Tendon cell contraction of collagen-GAG matrices in vitro: effect of cross-linking. *Biomaterials*. 21:1607–1619.
51. Moore, T. L., F. J. O'Brien, and L. J. Gibson. 2004. Creep does not contribute to fatigue in bovine trabecular bone. *J. Biomech. Eng*. 126: 321–329.
52. Flanagan, L. A., Y. E. Ju, B. Marg, M. Osterfield, and P. A. Janmey. 2002. Neurite branching on deformable substrates. *Neuroreport*. 13: 2411–2415.
53. Sethi, K. K., I. V. Yannas, V. Mudera, M. Eastwood, C. McFarland, and R. A. Brown. 2002. Evidence for sequential utilization of fibronectin, vitronectin, and collagen during fibroblast-mediated collagen contraction. *Wound Repair Regen*. 10:397–408.
54. Lutolf, M. P., and J. A. Hubbell. 2005. Synthetic biomaterials as instructive extracellular microenvironments for morphogenesis in tissue engineering. *Nat. Biotechnol*. 23:47–55.